Oral presentation | Numerical methods
Numerical methods-I
Tue. Jul 16, 2024 2:00 PM - 4:00 PM Room A

[5-A-04] An Efficient Conservative Primitive Solver for Non-Ideal Fluids in Single- and Multi-Phase Flows

*Giuseppe Sirianni[1], Barbara Re[1], Alberto Guardone[1], Remi Abgrall[2] (1. Politecnico di Milano, 2. University of Zurich)

Keywords: conservative, primitive, non-ideal, efficient

**Twelfth International Conference on
Computational Fluid Dynamics (ICCFD12),
Kobe, Japan, July 14-19, 2024**

Mixture-Conservative Temperature-Based Baer-Nunziato Solver for Efficient Full-Disequilibrium Simulations of Real Fluids

G. Sirianni*, B. Re* and R. Abgrall**
Corresponding author: giuseppe.sirianni@polimi.it
*Department of Aerospace Science and Technology, Politecnico di Milano, Via La Masa 34, 20156 Milano, Italy.
**Institute of Mathematics, Universität Zürich, Winterthurerstrasse 190, 8057 Zürich, Switzerland.

Abstract:
In this work we present a primitive update scheme for the full-disequilibrium Baer-Nunziato equations that is mixture total energy conservative and valid for generic equations of state. The update scheme is derived for a generic thermodynamic variable and is independent from the chosen spatial discretization. We show results of various Riemann problems from the literature obtained by updating phasic temperatures through the proposed scheme, and compare them to the standard approach and analytical solutions. Mixture total energy imbalance is assessed, and computational speed-ups using the Span-Wagner equation of state are briefly discussed. Finally, the scheme is tested in complex thermodynamic conditions on a two-phase non-ideal and a two-fluid non-classical Riemann problem, using the Span-Wagner equation of state with vanishing phases.

Keywords: Primitive formulation, Mixture conservative scheme, Non-ideal compressible fluid dynamics (NICFD), Span-Wagner equation of state, Baer-Nunziato, Two phase.

1 Introduction

Compressible multi-phase flows are ubiquitous in nature and are of great interest for many engineering applications such as nuclear power plants, steam turbines, and fuel injectors. Most of these systems are characterized by compressibility effects and complex thermodynamic behavior that requires expensive state-of-the-art thermodynamic models. In many cases, the effects of mechanical and thermal disequilibrium between the phases also play a major role in the behavior of these complex systems, hence the need for accurate and robust numerical tools able to model this kind of flow.

The Baer-Nunziato [1] (BN) model is widely used in the literature to describe compressible two-phase and two-fluid flows at both mechanical and thermal disequilibrium. The BN model can be split into a set of hyperbolic equations, on which we focus in this work, and a set of relaxation equations. The hyperbolic equations are historically written and solved for the two partial densities, momentums, total energies, and the volume fraction because the sum of these equations naturally yields conservation of the mixture density, momentum and total energy. Compared to the Euler equations for single-phase flows, the numerical solution of the BN model presents many additional difficulties. Firstly, it requires closures for the interfacial velocity and pressure [2, 3] present in the non-conservative terms that model interfacial interactions between phases. The numerical integration of these terms requires particular care to avoid spurious oscillations at material interfaces, namely it must preserve the pressure-velocity non-disturbance condition of Abgrall [4]. One of the main methods used to integrate the non-conservative terms is the path-conservative approach put forward by Pares & Castro. [5, 6]. This approach has been extensively applied to the BN equations and two-phase models, see for example [7, 8, 9, 10], but have been shown not to be capable of computing the correct solution of non-conservative systems [11, 12].

In addition to these numerical difficulties, solving the PDE system resulting from the BN model is intrinsically expensive due to the number of equations and the need for an equation of state (EoS) for each phase. Since the use of an accurate EoS is a common requirement for accurately modeling many engineering problems related to two-phase flows, particularly near saturation, metastable or critical conditions, the EoS evaluation can become a limiting factor. This is true for example for thermodynamic models such as the Span-Wagner (SW) EoS [13] when evaluated through density and energy, which are

the naturally available variables in a standard compressible BN solver. The tabulation of the EoS in so-called look-up tables (LUT) [14] has been widely adopted in the field of non-ideal compressible fluid dynamics (NICFD) [15] to decrease the computational burden. The LUT approach is based on a dataset containing the thermodynamic properties of a fluid computed in a pre-processing step, with an accurate but expensive EoS. During the simulation, the evaluation of the thermodynamic state is based on interpolation of these discrete data. Look-up tables have also been applied in simulation of two-phase flows with phase-transition [16, 17, 18]. However, thermodynamic stability and consistency are not guaranteed in standard LUT methods [19].

An alternative strategy to decrease the computational cost is to use a primitive formulation of the governing equations, namely in the natural variables in which the EoS is expressed. For instance, the multiparametric EoSs, such as SW EoS, are expressed in terms of density and temperature. If the governing equations are expressed in the conservative variables, the evaluation of the thermodynamic state requires solving a non-linear equation. On the contrary, if density and temperature are already available via the PDE integration, the evaluation of the thermodynamic state is straightforward and cheaper.

In the context of compressible two-phase flows, only some pressure formulations have been proposed. Some examples include a pressure formulation or the simplified Kapila model by Abgrall et al. [20], a single-pressure six equation model by Zhang et al. [21] and a full-disequilibrium pressure-based BN-type model by Re & Abgrall [22]. To the best of our knowledge, in the literature, there is no temperature-based formulation of the full-disequilibrium BN model. The non conservative nature of these formulations leads to errors in captured shock speeds and jump conditions. Thomann & Dumbser [23] have recently developed a numerical scheme for compressible two-phase flows that discretizes two entropy inequalities and obtains total energy conservation as a consequence of the thermodynamically compatible discretization proposed by Abgrall et al. [24]. Their scheme solves a symmetric hyperbolic and thermodynamically compatible (SHTC) model for two-phase flows [25, 26], which in the stiff relaxation limit tends to a BN-type model. However, it is currently limited to the polytropic ideal gas (PIG) assumption.

In a previous work focused on single-phase flows, the authors derived a primitive update scheme for the Euler equations under an arbitrary EoS [27] that conserves total energy, similarly to the residual correction approach presented by Abgrall [28]. Instead of the total energy, the scheme updates the primitive variable φ, which can be any thermodynamic variable, such as pressure, temperature, internal energy, entropy, or enthalpy. Notably, the primitive scheme that updates temperature instead of total energy led to a speed-up of up to 700% when using the SW EoS implemented through the thermodynamic library CoolProp [29].

Starting from these findings, in this work, we aim to extend this primitive update scheme to a full-disequilibrium BN solver. The idea is to advance the phasic temperatures instead of evolving the partial total energies, as usually done in standard BN solvers, preserving the conservation of the mixture total energy and minimizing the costs associated with accurate EoS, while avoiding thermodynamical inconsistencies possibly generated by look-up tables.

The structure of the paper is as follows. Section 2 describes the primitive update scheme of a generic phasic thermodynamic variables φ_k instead of updating the partial total energies. Section 3 presents the results of the temperature update scheme, that is with $\varphi_k = T_k$. We start showing the results of 1D Riemann problems from the literature using the PIG EoS in section 3.1. In section 3.2 we assess the pressure-velocity non-disturbance condition [4] using the SW EoS and briefly discuss computational costs. Throughout these first two sections we assess the imbalance of mixture total energy in time. In section 3.3, the spatial convergence order is measured using the method of manufactured solutions [30] using the polytropic van der Waals (vdW) EoS [31]. Then, to assess the behavior of the scheme when complex thermodynamic behavior is dominant, in section 3.4 we present one two-phase non-ideal [15] and one two-fluid non-classical [32, 33, 34] Riemann problem with vanishing phases using the SW EoS, with instantaneous mechanical relaxation. Finally, we draw conclusions in section 4.

2 Numerical scheme

The hyperbolic part of the full-disequilibrium BN model for phases $k = 1, 2$ reads

$$\frac{\partial}{\partial t}\begin{bmatrix}\alpha_k\\ \alpha\rho_k\\ \alpha\rho\boldsymbol{u}_k\\ \alpha E_k^t\end{bmatrix} + \nabla\cdot\begin{bmatrix}\boldsymbol{0}\\ \alpha\rho\boldsymbol{u}_k\\ \alpha_k\left(\rho\boldsymbol{u}_k\otimes\boldsymbol{u}_k + P_k\boldsymbol{I}\right)\\ \alpha_k\left(E_k^t + P_k\right)\boldsymbol{u}_k\end{bmatrix} + \begin{bmatrix}\boldsymbol{u}_I\\ \boldsymbol{0}\\ -P_I\boldsymbol{I}\\ -P_I\boldsymbol{u}_I\end{bmatrix}\cdot\nabla\alpha_k = \boldsymbol{0}. \tag{1}$$

We define the vector of evolution variables $\boldsymbol{q}_k = [\alpha_k, \alpha\rho_k, \alpha\rho\boldsymbol{u}_k, \alpha E_k^t]$, which is composed of the volume fraction and the partial density, momentum, and total energy, respectively[1]. We also define the phasic pressures P_k, temperatures T_k, and internal energies per unit volume E_k. We use the original Baer-Nunziato [1] closure for the interfacial velocity $\boldsymbol{u}_I = \boldsymbol{u}_2$ and interfacial pressure $P_I = P_1$. The system of Eqs. (1) is closed by a thermodynamic model for each phase (or fluids) and the saturation condition $\alpha_1 + \alpha_2 = 1$.

The BN Eqs. (1) cannot be written in conservative (or divergence) form, because of the non-conservative product involving the gradient of the volume fraction. By summing Eqs. (1) over phases k, the non-conservative terms containing $\nabla\alpha_k$ cancel out and we retrieve the Euler conservation equations for the mixture density ρ_m, momentum $\rho\boldsymbol{u}_m$ and total energy E_m^t, with $P_m = \alpha_1 P_1 + \alpha_2 P_2$ being the mixture pressure. We can rewrite the BN Eqs. (1) in a more compact form including the evolution variables of both phases in the vector $\boldsymbol{q} = [\alpha_1, \alpha\rho_1, \alpha\rho\boldsymbol{u}_1, \alpha E_1^t, \alpha\rho_2, \alpha\rho\boldsymbol{u}_2, \alpha E_2^t]$ and noting that $\nabla\alpha_1 = -\nabla\alpha_2$

$$\frac{\partial\boldsymbol{q}}{\partial t} + \nabla\cdot\boldsymbol{F}(\boldsymbol{q}) + \boldsymbol{G}(\boldsymbol{q})\cdot\nabla\alpha_1 = \boldsymbol{0}, \tag{2}$$

where $\boldsymbol{F}(\boldsymbol{q})$ are the conservative fluxes and $\boldsymbol{G}(\boldsymbol{q})\cdot\nabla\alpha_1$ the non-conservative terms. After applying the divergence theorem, the integral form of Eq. (2) in domain Ω reads

$$\int_\Omega \frac{\partial\boldsymbol{q}}{\partial t}dV + \oint_{\partial\Omega}\boldsymbol{F}(\boldsymbol{q})\cdot\hat{\boldsymbol{n}}dA + \int_\Omega \boldsymbol{G}(\boldsymbol{q})\cdot\nabla\alpha_1 dV = \boldsymbol{0}, \tag{3}$$

where $\hat{\boldsymbol{n}}$ is the outward unit vector normal to the domain boundary $\partial\Omega$. By discretizing the domain Ω in finite volumes C_i and using forward Euler time integration from time t^n to t^{n+1}, we write the time-discrete version of Eq. (3) as

$$\sum_{C_i\in\Omega}\left[\int_{C_i}\left(\frac{\boldsymbol{q}_i^{n+1} - \boldsymbol{q}_i^n}{\Delta t}\right)dV + \oint_{\partial C_i}\boldsymbol{F}(\boldsymbol{q}^n)\cdot\hat{\boldsymbol{n}}dA + \int_{C_i}\boldsymbol{G}(\boldsymbol{q}^n)\cdot\nabla\alpha_1 dV\right] = \boldsymbol{0}. \tag{4}$$

We define the discretized residual $\boldsymbol{\Phi}_i$ of the BN equations on a finite volume C_i as

$$\boldsymbol{\Phi}_i(\boldsymbol{q}^n) \simeq \oint_{\partial C_i}\boldsymbol{F}(\boldsymbol{q}^n)\cdot\hat{\boldsymbol{n}}dA + \int_{C_i}\boldsymbol{G}(\boldsymbol{q}^n)\cdot\nabla\alpha_1 dV. \tag{5}$$

The previous expression encompasses the spatial discretization of the governing equations. We integrate the convective fluxes and non-conservative terms using the HLLC-type Riemann solver with approximated two-phase contact by Lochon et al. [35], which allows the use of arbitrary equations of state and integrates the non-conservative products using the thin layer approximation [36] which enforces the pressure-velocity non-disturbance condition [4]. To achieve second-order accuracy in space, we employ the reconstruction procedure of Schwendeman [36] in conjunction with the slope limiter of Barth & Jespersen [37]. While doing this, we reconstruct primitives $\boldsymbol{p}^n = [\alpha_1, \rho_k, \boldsymbol{u}_k, P_k]$ instead of the evolution variables $\boldsymbol{q}^n$ to preserve the pressure-velocity non-disturbance condition.

We now drop the summation on $C_i \in \Omega$ in Eq. (4) and focus on the discrete balance for a single finite volume C_i, with the discrete space integrals defined in the right-hand side of Eq. (5). The forward Euler time integration scheme deriving from Eq. (4) and Eq. (5) for a single finite volume C_i simply reads

$$\boldsymbol{q}_i^{n+1} = \boldsymbol{q}_i^n - \frac{\Delta t}{C_i}\boldsymbol{\Phi}_i(\boldsymbol{q}^n). \tag{6}$$

[1]When subscript $(\cdot)_k$ is applied to a group of variables starting with α, it refers to all variables in that group, for example $\alpha\rho\boldsymbol{u}_k = \alpha_k\rho_k\boldsymbol{u}_k$

Analogously to what was done for single-phase flows in [27], we use the previous expression to directly update the volume fraction, partial densities, and partial momentums, whereas, as described below, we proceed differently for partial total energies.

2.1 Primitive update for the partial total energy equations

In this subsection, we illustrate the update strategy based on the phasic primitive variable φ_k that replaces the direct updates of the partial total energies in Eq. (6). To ease the notation, we drop the subscript $(\cdot)_i$ as we now focus on a single finite volume. We drop also the subscript $(\cdot)_k$ as all equations here refer to the phase k.

Assume that the EoS for the phase k can be expressed in the form $E = E(\rho, \varphi)$, where, as said in the introduction, φ is a thermodynamic variable arbitrarily chosen among $[T, P, e, s, h]$, where the last three variables are, respectively, phasic the internal energy, entropy, and enthalpy per unit of mass. The partial total energy is defined as

$$\alpha E^t = \alpha E(\rho, \varphi) + \frac{1}{2}\alpha\rho\boldsymbol{u}^2. \tag{7}$$

By summing and subtracting $\alpha^{n+1}E^n$ to (7), we can write the time-discrete jump of partial total energy as

$$\begin{aligned}\Delta(\alpha E^t) = \Delta(\alpha E) + \frac{1}{2}\Delta(\alpha\rho\boldsymbol{u}^2) &= \left[\alpha^{n+1}E^{n+1} - \alpha^n E^n + \left(\alpha^{n+1}E^n - \alpha^{n+1}E^n\right)\right] + \frac{1}{2}\Delta(\alpha\rho\boldsymbol{u}^2) \\ &= \alpha^{n+1}\Delta E + E^n\Delta\alpha + \frac{1}{2}\Delta(\alpha\rho\boldsymbol{u}^2).\end{aligned} \tag{8}$$

where the jump in the phasic internal energy ΔE is the only unknown term. The time derivative of the phasic internal energy can be written in terms of its thermodynamic derivatives $E_{\varphi,\rho} = \left(\frac{\partial E}{\partial \varphi}\right)_\rho$ and $E_{\rho,\varphi} = \left(\frac{\partial E}{\partial \rho}\right)_\varphi$ as

$$\frac{\partial E}{\partial t} = E_{\varphi,\rho}\frac{\partial \varphi}{\partial t} + E_{\rho,\varphi}\frac{\partial \rho}{\partial t}. \tag{9}$$

Integrating Eq. (9) between t^n and t^{n+1} and assuming $E_{\varphi,\rho} = \overline{E_{\varphi,\rho}}$ and $E_{\rho,\varphi} = \overline{E_{\rho,\varphi}}$ constants, we derive an approximation for ΔE:

$$\Delta E^{\text{appr}} \simeq \overline{E_{\varphi,\rho}}\Delta\varphi + \overline{E_{\rho,\varphi}}\Delta\rho \tag{10}$$

which can be substituted into Eq. (8), yielding

$$\Delta\alpha E^t \simeq \alpha^{n+1}\left(\overline{E_{\varphi,\rho}}\Delta\varphi + \overline{E_{\rho,\varphi}}\Delta\rho\right) + E^n\Delta\alpha + \frac{1}{2}\Delta(\alpha\rho\boldsymbol{u}^2). \tag{11}$$

In Eq. (11) there are two distinct contributions to the jump of partial total energy: a term containing an approximation of the jump of phasic internal energy ΔE^{appr}, and two terms containing the exact jumps of volume fraction and partial kinetic energy respectively. These last two terms are known exactly since the volume fraction, partial densities and partial momentums have been already updated using Eq (6).

We can use Eq. (11) to write the discrete version of the partial total energy equation in the finite volume C as

$$\int_C \left(\alpha^{n+1}\left(\overline{E_{\varphi,\rho}}\Delta\varphi + \overline{E_{\rho,\varphi}}\Delta\rho\right) + E^n\Delta\alpha + \frac{1}{2}\Delta(\alpha\rho\boldsymbol{u}^2)\right) dV + \Delta t\,\Phi^{\alpha E^t} = 0. \tag{12}$$

We can isolate the term containing $\Delta\varphi$ from Eq. (12) and rename it B for simplicity

$$\underbrace{\int_C \alpha^{n+1}\overline{E_{\varphi,\rho}}\Delta\varphi dV}_{B} + \int_C \left(\alpha^{n+1}\overline{E_{\rho,\varphi}}\Delta\rho + E^n\Delta\alpha + \frac{1}{2}\Delta(\alpha\rho\boldsymbol{u}^2)\right) dV + \Delta t\,\Phi^{\alpha E^t} = 0. \tag{13}$$

Using the forward Euler time update scheme Eq. (6) for the generic thermodynamic variable φ, we

define a pseudo-spatial residual Φ^φ in the finite volume C as

$$\varphi^{n+1} = \varphi^n - \frac{\Delta t}{C}\,\Phi^\varphi \quad \rightarrow \quad \Delta\varphi = -\frac{\Delta t}{C}\,\Phi^\varphi. \tag{14}$$

The residual Φ^φ exactly satisfies the approximate partial total energy equation Eq. (12). Substituting Eq. (14) into the definition of B, we obtain

$$B = \int_C \alpha^{n+1}\overline{E_{\varphi,\rho}}\left(-\frac{\Delta t}{C}\,\Phi^\varphi\right) dV = -\Delta t\,\Phi^\varphi \underbrace{\frac{1}{C}\int_C \alpha^{n+1}\overline{E_{\varphi,\rho}} dV}_{\overline{\omega}} = -\Delta t\,\Phi^\varphi\overline{\omega}. \tag{15}$$

Plugging this new expression for B back into Eq. (13), we get

$$-\Delta t\,\Phi^\varphi\overline{\omega} + \int_C \left(\alpha^{n+1}\overline{E_{\rho,\varphi}}\Delta\rho + E^n\Delta\alpha + \frac{1}{2}\Delta(\alpha\rho\boldsymbol{u}^2)\right) dV + \Delta t\,\Phi^{\alpha E^t} = 0. \tag{16}$$

We can invert this expression to find an equation for the pseudo-spatial residual Φ^φ for the generic phasic thermodynamic variable φ. This, together with the update formula Eq. (14), finally yields:

$$\begin{cases} \Phi^\varphi = \dfrac{1}{\overline{\omega}\Delta t}\left[\displaystyle\int_C \left(\alpha^{n+1}\overline{E_{\rho,\varphi}}\Delta\rho + E^n\Delta\alpha + \frac{1}{2}\Delta(\alpha\rho\boldsymbol{u}^2)\right) dV + \Delta t\Phi^{\alpha E^t}\right] \\ \varphi^{n+1} = \varphi^n - \dfrac{\Delta t}{C}\Phi^\varphi\,. \end{cases} \tag{17}$$

As mentioned, $\Delta\alpha$, $\Delta\rho$ and $\Delta(\alpha\rho\boldsymbol{u}^2)$ in Eq. (17) are exactly known from Eq. (6). Contrarily, Φ^φ, and consequently φ^{n+1}, are all functions of the approximate unknowns $\overline{E_{\varphi,\rho}}$ and $\overline{E_{\rho,\varphi}}$. From here on, the scheme is identical to that presented in [27], but we summarize it here for convenience. We move the unknowns from $\overline{E_{\varphi,\rho}}$ and $\overline{E_{\rho,\varphi}}$ to $\overline{\rho}$ and $\overline{\varphi}$ by assuming

$$\begin{cases} \overline{E_{\varphi,\rho}} = E_{\varphi,\rho}(\overline{\rho},\overline{\varphi}) \\ \overline{E_{\rho,\varphi}} = E_{\rho,\varphi}(\overline{\rho},\overline{\varphi})\,. \end{cases} \tag{18}$$

We then define $\overline{\rho} = \left(\rho^{n+1} + \rho^n\right)/2$ as we already know the updated phasic densities so that the problem is now limited to a single unknown $\overline{\varphi}$. Using Eq. (17) and (18), we define $\varphi^{n+1}(\overline{\varphi})$ and use it to compute both the approximate internal energy jump as defined in Eq. (10) and the thermodynamically exact jump through the EoS, namely

$$\begin{cases} \Delta E^{\text{appr}}(\overline{\varphi}) = \overline{E_{\varphi,\rho}}(\overline{\rho},\overline{\varphi})\Delta\varphi(\overline{\varphi}) + \overline{E_{\rho,\varphi}}(\overline{\rho},\overline{\varphi})\Delta\rho \\ \Delta E^{\text{tmd}}(\overline{\varphi}) = E(\rho^{n+1},\varphi^{n+1}(\overline{\varphi})) - E(\rho^n,\varphi^n)\,. \end{cases} \tag{19}$$

As previously mentioned, the partial kinetic energy jump has already been computed from Eq. (6). Therefore, if the approximate and thermodynamic internal energy jumps coincide, the approximate jump of partial total energy Eq. (11) will be equal to the exact one that would result from applying Eq. (6) to the partial total energy equation. We can define a scalar function $F(\overline{\varphi})$ such that this condition is met, namely

$$F(\overline{\varphi}) = \frac{\Delta E^{\text{tmd}}(\overline{\varphi}) - \Delta E^{\text{appr}}(\overline{\varphi})}{E(\rho^n,\varphi^n)}. \tag{20}$$

We then apply a root searching algorithm to find $\overline{\varphi}$ such that $F(\overline{\varphi}) = 0$. As done in [27], in this work, we use the secant root search algorithm with a tolerance of $|F(\overline{\varphi}_{(k)})| < tol = 10^{-12}$. Note that we dropped the subscripts $(\cdot)_k$ and $(\cdot)_i$, but the scheme has to be applied independently for $k = 1, 2$, at each finite volume. Hence, we solve the equation $F(\overline{\varphi}) = 0$ twice for all finite volumes $C_i \in \Omega$.

The procedure described in this section is in principle valid for any choice of the phasic thermodynamic variable $\varphi = [P, T, e, s, h]$. However, we limit ourselves to using the temperature, i.e., $\varphi = T$, due to the computational cost benefits measured in [27] when using the SW EoS [13].

		Left $x < 0.5$ m		**Right** $x \geq 0.5$ m	
		Phase 1	**Phase 2**	**Phase 1**	**Phase 2**
α	[−]	0.9	0.1	0.8	0.2
ρ	[kg/m^3]	0.5806	0.2068	0.4890	2.2263
u	[m/s]	1.5833	1.4166	−0.70138	0.9366
P	[Pa]	1.375	0.0416	0.986	6

Table 1: Coinciding shocks-rarefactions test from [38]: initial conditions.

3 Results

In this section, we present a number of 1D test cases to assess the proposed primitive update scheme with $\varphi_k = T_k$. Firstly, in section 3.1 we show results on various 1D Riemann problems from Adrianov & Warnecke [38]. In section 3.2, we check the pressure-velocity non-disturbance condition [4] in a volume fraction advection test using the SW EoS [13] through the CoolProp thermodynamic library [29]. Throughout these first two sections, we will compare the proposed temperature update scheme (T update) to the standard partial total energy update (αE^t update), and provide time plots of the dimensionless mixture total energy imbalance $I^{E^t_m}(t)$, which is defined as

$$I^{E^t_m}(t) = \frac{1}{C_\Omega \cdot \int_\Omega E^t_m(0) dV} \Bigg\{ \left[\int_\Omega E^t_m(\tau) dV \right]_{\tau=t} - \left[\int_\Omega E^t_m(\tau) dV \right]_{\tau=0} + \int_{\tau=0}^{\tau=t} \left[\oint_{\partial\Omega} \sum_{k=1}^{2} \boldsymbol{F}^{\alpha E^t_k}(\tau) \cdot \hat{\boldsymbol{n}} dA \right] d\tau \Bigg\}. \tag{21}$$

Note that the non-conservative terms containing $\nabla \alpha_k$ in Eq. (1) do not appear in Eq. (21) because their sum over phases $k = 1, 2$ cancels out by definition. In section 3.3, we use the method of manufactured solutions (MMS) [30] and the vdW EoS to check that the order of convergence of the underlying spatial discretization is retained. In section 3.4, we present two Riemann problems with a vanishing phase using the SW EoS and instantaneous mechanical relaxation [39], modeled through pressure and velocity relaxation source terms in the volume fraction, partial momentum and partial total energy equations. These are designed to showcase the robustness of the method in the non-ideal [15] and non-classical [32, 33, 34] regimes.

3.1 Riemann problems - Mixture conservation

Here, we present three Riemann problems from Adrianov & Warnecke [38] to compare the proposed scheme, labeled "T update", to the standard scheme that solves the total energy equations, labeled "αE^t update", and exact solutions. Both phases are modeled under the polytropic ideal gas (PIG) assumption, with the specific heat ratio $\gamma = 1.4$. In all three cases, the domain is $x \in [0, 1]$ m, which is discretized over a uniform grid with $\Delta x = 2.5$ mm. The initial position of the discontinuity is $x = 0.5$ mm. The results are shown at time $t_{final} = 0.1$ s, reached using a variable time step satisfying $CFL = 0.1$, that is

$$\Delta t = \max_{C_i \in \Omega} \left\{ \frac{CFL \cdot C_i}{\sum_{C_j \in \partial C_i} \left[A_{i,j} \lambda^{\max}_{i,j} \right]} \right\} \qquad \text{with} \qquad \lambda^{\max}_{i,j} = \max_k \left(\frac{|\boldsymbol{u}_{k,i} \cdot \hat{\boldsymbol{n}}| + c_{k,i} + |\boldsymbol{u}_{k,j} \cdot \hat{\boldsymbol{n}}| + c_{k,j}}{2} \right) \tag{22}$$

The first test, see table 1 for the initial conditions and Fig. 1 for the results, features a compression shock in phase 1 that is located within a rarefaction fan in phase 2. This wave configuration is used to test if the scheme able to handle different coinciding waves in the two phases without introducing spurious interactions. The plots of the phasic densities, pressures and the volume fraction in Fig. 1 show great overall agreement with the analytical solution, with no evident oscillations in either phase across the shock in phase 1 located at $x \simeq 0.7$ m. A kink in the density of phase 2 can be seen across the two-phase contact located at $x \simeq 0.45$ m, a similar numerical artifact to that visible in Fig. 8 in Adrianov & Warnecke [38] using the VFRoe scheme [40].

The second test, see table 2 for the initial data and Fig. 2 for the results, presents a rarefaction fan

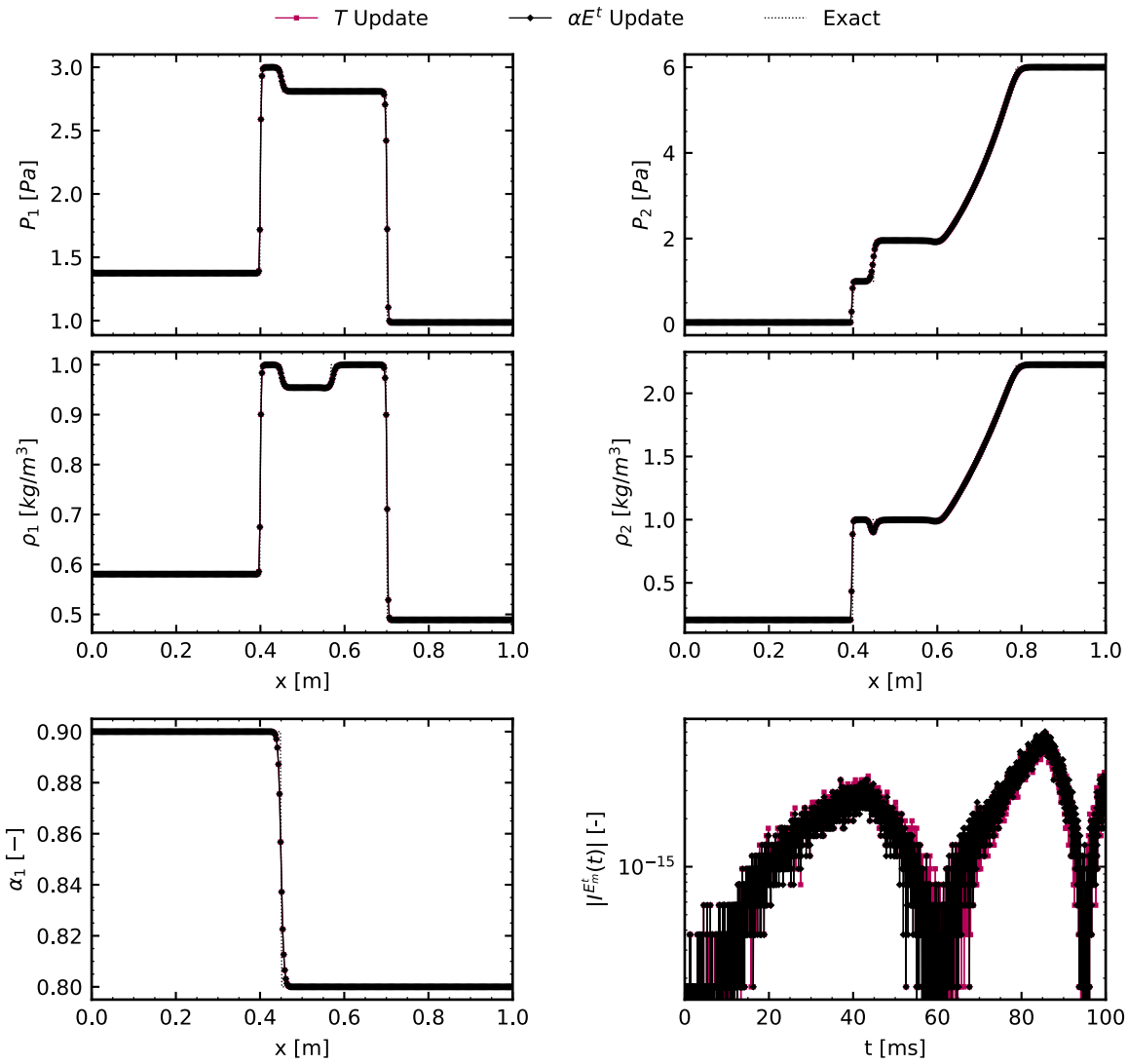

Figure 1: Coinciding shocks-rarefactions test results using PIG EoS. Phasic pressures, densities, and volume fraction are plotted at $t = 0.1$s, along with the absolute value of the dimensionless mixture total energy imbalance in time. The results of the proposed T update scheme, the standard αE^t update, and the exact solution from Adrianov & Warnecke [38] are compared.

		Left $x < 0.5$ m		**Right** $x \geq 0.5$ m	
		Phase 1	**Phase 2**	**Phase 1**	**Phase 2**
α	[−]	0.5	0.5	0.9	0.1
ρ	[kg/m^3]	0.2702	2	0.4666	1
u	[m/s]	−3.4016	−1	−2.6667	−1
P	[Pa]	0.1	2	0.2148	8.3994

Table 2: Rarefaction attached to contact test from [38]: initial conditions.

		Left $x < 0.5$ m		**Right** $x \geq 0.5$ m	
		Phase 1	**Phase 2**	**Phase 1**	**Phase 2**
α	[−]	0.9	0.1	0.1	0.9
ρ	[kg/m^3]	2.6718	0.9123	1.3359	0.8592
u	[m/s]	−0.050	1.6305	0.5438	−0.0129
P	[Pa]	1.5	1.5666	1.5	1.1675

Table 3: Coinciding contacts test from [38]: initial conditions.

in phase 1 that approaches, from the left, the two-phase contact located at $x \simeq 0.4$ m. This generates a parabolic degeneracy in the BN system as the rightmost characteristic of the fan approaches the two-phase contact speed, see section 8.3 in [38] for details. Results for both the phasic pressures, the phase 1 velocity, and the phase 1 volume fraction agree well with the exact solution, with some spurious oscillations away from the two-phase contact being present. The velocity of phase 2 presents significant oscillations whereas it should be constant. The overall behavior of all variables is consistent with the numerical results of Adrianov & Warnecke [38] using the VFRoe scheme [40].

The third test, see table 3 for the initial conditions and Fig. 3 for the results, presents two coinciding contacts for the two phases at $x \simeq 0.52$ m. In this test, all variables reached a great agreement between the exact and numerical solutions.

For all three tests, the results for the T update scheme and the standard αE^t update scheme are superimposed in all variables. Looking at the absolute values of the dimensionless mixture total energy imbalance for all three tests in Figs. 1 2 3, there is no appreciable loss in conservation of mixture total energy when using the T update scheme compared to the standard αE^t update.

3.2 Volume fraction advection - Non-disturbance condition

This test represents the advection at constant velocity of a bubble of nitrogen in a tube of carbon dioxide. The main goal is to show that the non-disturbance condition for compressible two-phase flows [4] is met. Phase 1 is nitrogen (N_2 [41]) and phase 2 is carbon dioxide (CO_2 [42]), both fluids are modeled using the SW EoS implemented through the thermodynamic library CoolProp [29].

The domain is $x \in [0, 10]$ m and the initial position of the bubble is $x \in [1, 3]$ m, where the fluid is 99% of nitrogen ($\alpha_1 = 0.99$). Elsewhere, the fluid is 99% carbon dioxide ($\alpha_2 = 0.99$). The domain is split into 400 uniform cells ($\Delta x = 25$ mm). The test conditions are given in table 4. The results are computed at the final time $t_{final} = 0.1$ s, imposing a $CFL = 0.1$.

Plots of phasic pressures, velocities, and volume fraction are in Fig. 4. The constant initial pressure-velocity field is preserved after the two-phase contact moves right at the correct speed. Furthermore, the absolute value of the dimensionless total energy balance in time in Fig. 4 is close to machine precision $\epsilon_{\text{machine}} \simeq 10^{-16}$ for both the T update and the standard αE^t update, although their time plots are slightly different. We measured the CPU time per iteration in table 5 and the corresponding speed-up is roughly 440%, confirming the expected cost decrease but with worse results than the value of 700% measured for the single-phase scheme in [27]. This is caused by the need to reconstruct phasic pressures instead of phasic temperatures to preserve the pressure-velocity non-disturbance condition [4], negating some of the computational cost savings that reconstructing phasic temperatures would yield.

3.3 Order testing - Method of manufactured solutions

In this section, we use the method of manufactured solutions [30] (MMS) to demonstrate that the order of convergence of the underlying spatial discretization is preserved. The underlying idea is to simply generate an exact solution that need not be physically meaningful. We assume periodic boundary

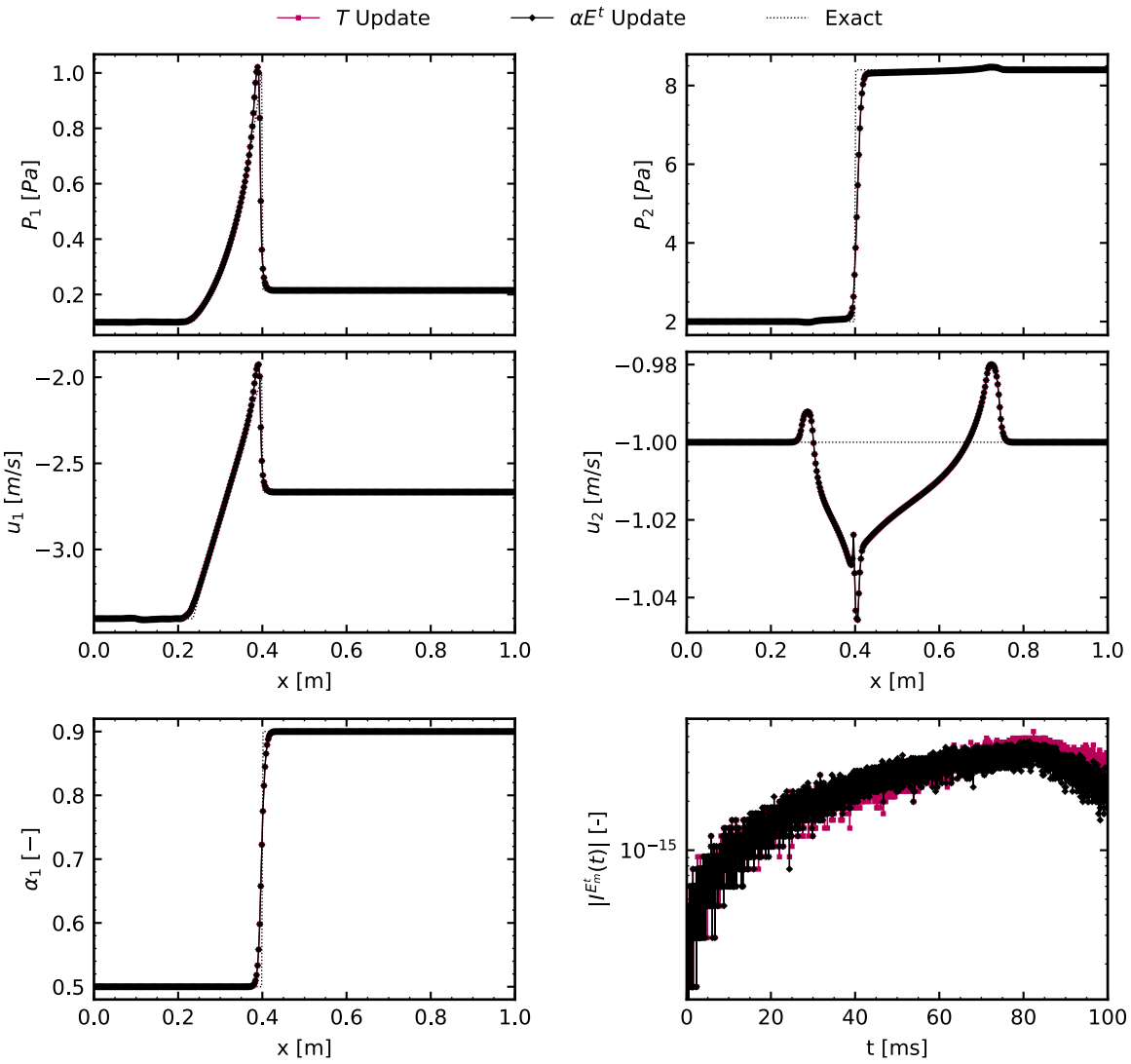

Figure 2: Rarefaction attached to contact test: results using the PIG EoS. Phasic pressures, velocities, and volume fraction are plotted at $t = 0.1$s, along with the absolute value of the dimensionless mixture total energy imbalance in time. The results of the proposed T update scheme, the standard αE^t update, and the exact solution from Adrianov & Warnecke [38] are compared.

		Bubble $x \in [1,3]$ m		**Free-stream** $x \notin [1,3]$ m	
		Phase 1	**Phase 2**	**Phase 1**	**Phase 2**
α	[−]	0.99	0.01	0.01	0.99
ρ	[kg/m^3]	1.1458	1.1458	1.1458	1.1458
u	[m/s]	300	300	300	300
P	[Pa]	101325	101325	101325	101325

Table 4: Volume fraction advection test with the Span-Wagner equation of state: initial conditions.

		T Update	αE^t Update
Average iteration time	[s/it]	0.0262685	0.116279
Speed-up factor	[%]	442.65	100

Table 5: Average computational time per iteration and speed-up factor for the volume fraction advection test with the Span-Wagner equation of state. Comparison between the T update scheme and the standard αE^t update.

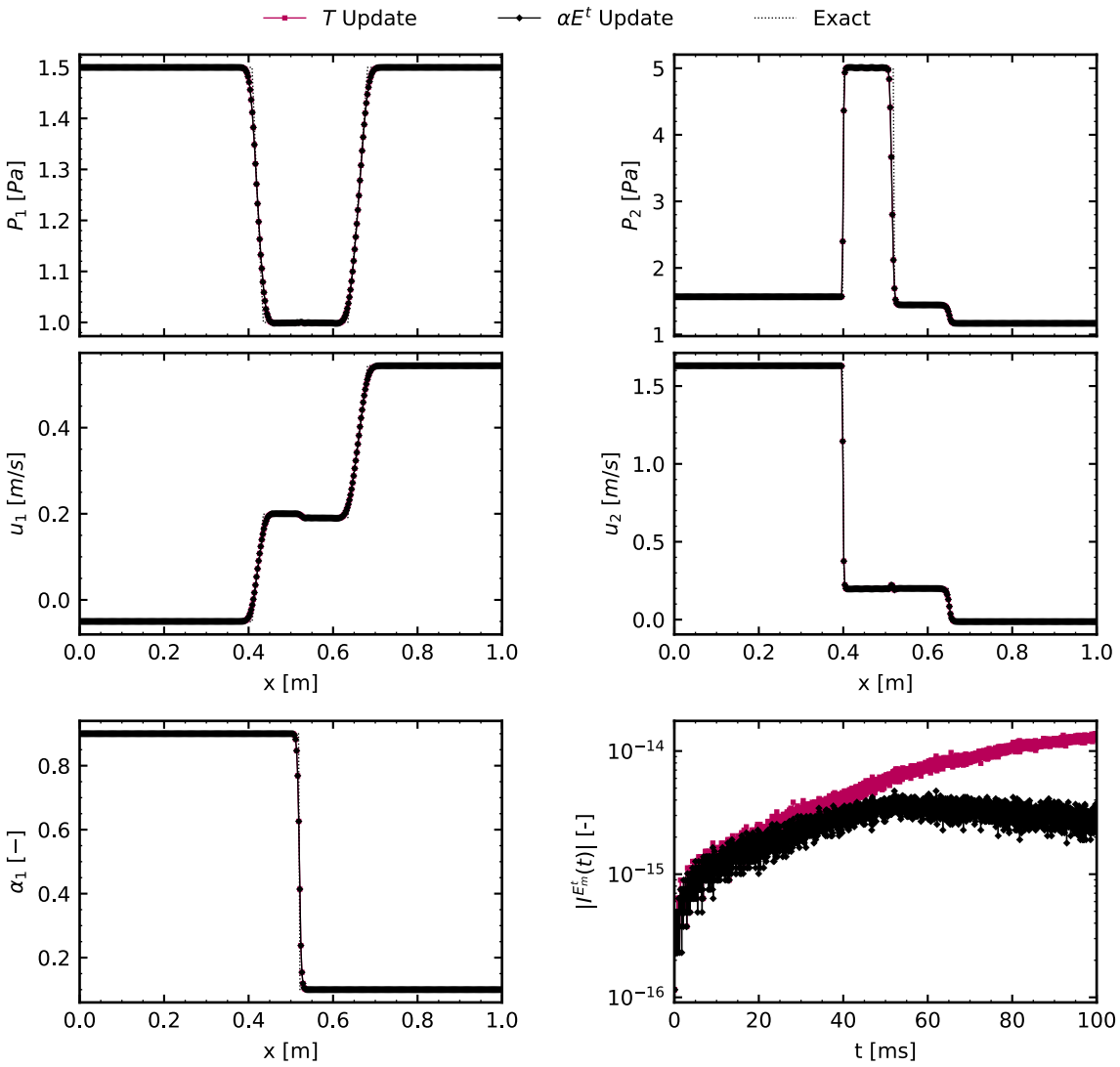

Figure 3: Coinciding contacts test: results using the PIG EoS. Phasic pressures, velocities, and volume fraction are plotted at $t = 0.1$s, along with the absolute value of the dimensionless mixture total energy imbalance in time. The results of the proposed T update scheme, the standard αE^t update, and the exact solution from Adrianov & Warnecke [38] are compared.

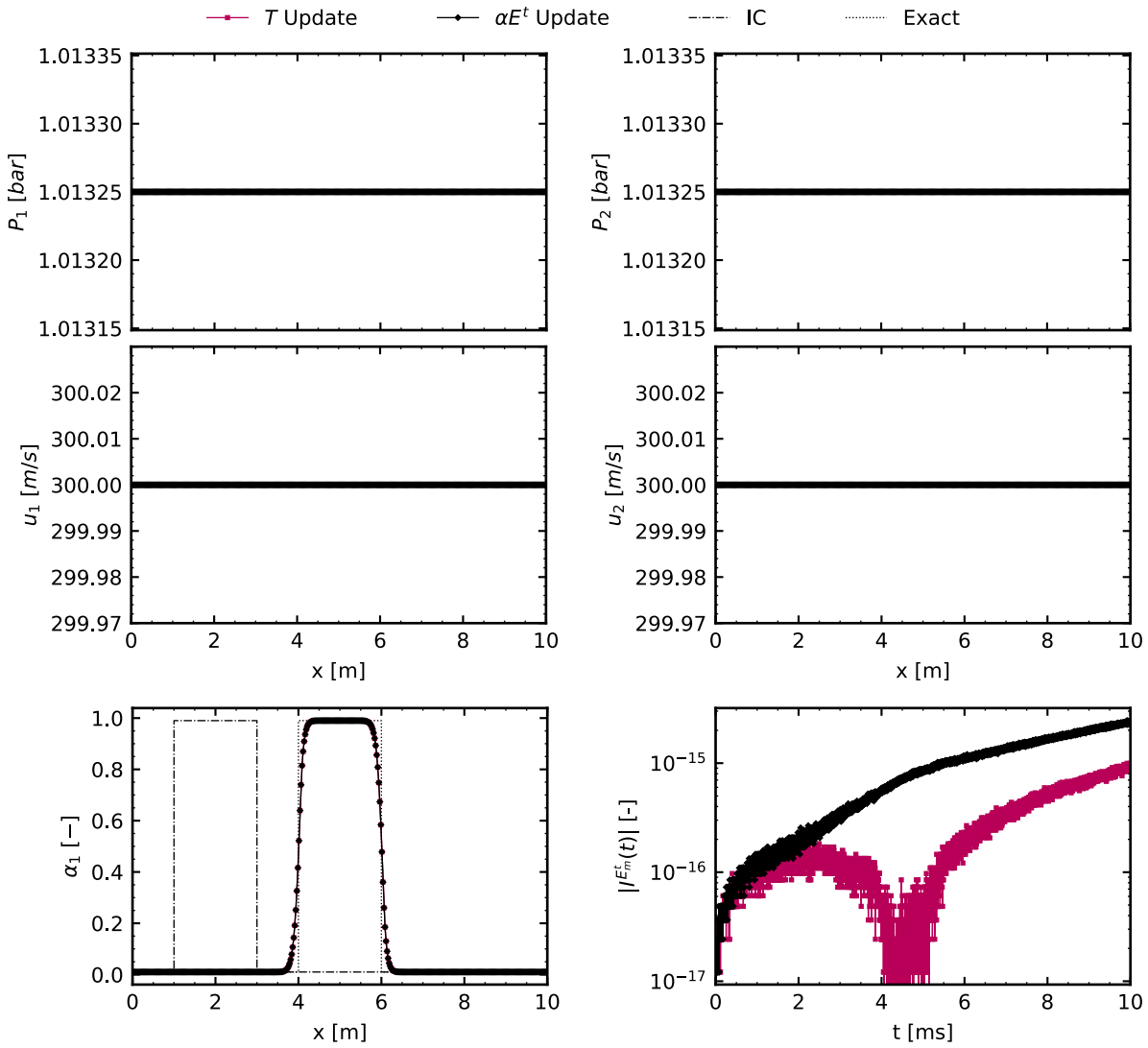

Figure 4: Volume fraction advection test with the Span-Wagner equation of state, results using the Coolprop [29] thermodynamic library. Phasic pressures, velocities, and volume fraction are plotted at $t = 0.01$s, along with the absolute value of the dimensionless mixture total energy imbalance in time. The results of the T update scheme are compared to the ones with the standard αE^t update.

		Phase 1 (vdW)	**Phase 2** (vdW)
γ	$[-]$	1.4	1.35
R	$[\mathrm{kJ/kg \cdot K}]$	327	302
a	$[\mathrm{s^2/m^2}]$	1.370	1.570
b	$[\mathrm{kg/m^3}]$	0.0387	0.014

Table 6: MMS test: thermodynamic data for the vdW Eos of both phases.

conditions in the domain $\Omega = [0, 1]$ m and modeled both fluids under the polytropic van der Waals equation of state with the parameters defined in table 6.

We define the exact manufactured solution as

$$\boldsymbol{p}^{\mathrm{MMS}}(x,t) = \begin{cases} \alpha_1^{\mathrm{MMS}}(x,t) &= \alpha_1^0 + A_{\alpha_1}\cos\left(\omega_x x + \omega_t t\right) \\ \rho_k^{\mathrm{MMS}}(x,t) &= \rho_k^0 + A_{\rho_k}\cos\left(\omega_x x + \omega_t t\right) \\ u_k^{\mathrm{MMS}}(x,t) &= u_k^0 + A_{u_k}\sin\left(\omega_x x + \omega_t t\right) \\ T_k^{\mathrm{MMS}}(x,t) &= T_k^0 + A_{T_k}\sin\left(\omega_x x + \omega_t t\right) \end{cases} \tag{23}$$

and substitute it into the Baer-Nunziato hyperbolic operator Eq. (1) to compute the MMS source terms that, when added to the BN equations, gives the exact solution $\boldsymbol{p}^{\mathrm{MMS}}(x,t) =$. We then compute the solution at time $t = 0.5$ ms with these source terms using $\omega_x = 2\pi$ m^{-1}, $\omega_t = 16\pi$ s^{-1} and the following constants

$$\begin{aligned} &\alpha_1^0 = 0.5 && A^{\alpha_1} = 0.25 \\ &\rho_1^0 = 2\ \mathrm{kg/m^3} && A^{\rho_1} = 0.025\ \mathrm{kg/m^3} \\ &u_1^0 = 100\ \mathrm{m/s} && A^{u_1} = 0.25\ \mathrm{m/s} \\ &T_1^0 = 300\ \mathrm{K} && A^{T_1} = 0.35\ \mathrm{K} \\ &\rho_2^0 = 1.8\ \mathrm{kg/m^3} && A^{\rho_2} = 0.08\ \mathrm{kg/m^3} \\ &u_2^0 = 125\ \mathrm{m/s} && A^{u_2} = 0.15\ \mathrm{m/s} \\ &T_2^0 = 320\ \mathrm{K} && A^{T_2} = 0.35\ \mathrm{K}\,. \end{aligned} \tag{24}$$

The L_2 norm of the dimensionless errors and the measured convergence rates are plotted in Fig. 5 for both phases, with and without the Schwendeman [36] reconstruction. Results confirm the expected first- and second-order rates of convergence in all variables for both phases.

3.4 Non-ideal and non-classical vanishing phase Riemann problems

In this section, we show two Riemann problems with vanishing phases, modeling the fluids under the SW EoS [13] through the thermodynamic library CoolProp [29] and the proposed T update scheme. For these tests, differently from the rest of the paper, we consider the BN model with mechanical relaxations, namely with additional source terms proportional to the pressure and velocity jumps between the two phases. The source terms are solved through the finite relaxation solver of Chiocchetti & Muller [39]. We set sufficiently large values (10^{11}) for the pressure and velocity relaxation parameters to mimic instantaneous mechanical relaxation.

The first test involves two siloxanes in the non-ideal compressible regime. The left state is almost pure MM (Hexamethyldisiloxane) vapour at higher pressure moving toward left, and the right state is almost pure MM liquid at rest. See table 7 for the initial data. The resulting wave configuration is sketched in Fig. 6 and is composed of a left-running rarefaction fan in the vapour phase, a two-phase contact separating the vapour and the liquid phases, and a right-running compression shock in the liquid phase. The comparison between the numerical results for the volume fraction, mixture pressure, density, and velocity in Fig. 7 show great agreement with the exact solution. Note that there is a point that appears to be falling inside the saturation curve for the numerical solution: actually, no pair (ρ_1, P_1) or (ρ_2, P_2) of the phasic solutions reaches metastable conditions. This is a "post-processing artifact" that occurs because, across the numerically diffused two-phase contact, a single point of the mixture solution (ρ_m, P_m) is inside the two-phase region, with $\rho_m = \alpha\rho_1 + \alpha\rho_2$ and $P_m = \alpha_1 P_1 + \alpha_2 P_2$.

The second and final test is a non-classical [32, 33, 34] two-fluid Riemann problem with pure MD_4M (Tetradecamethylhexasiloxane) vapour in the left state and pure Toluene vapour in the right state, see table 8 for the data. The resulting wave structure is sketched in Fig. 8 and is composed of a left-running

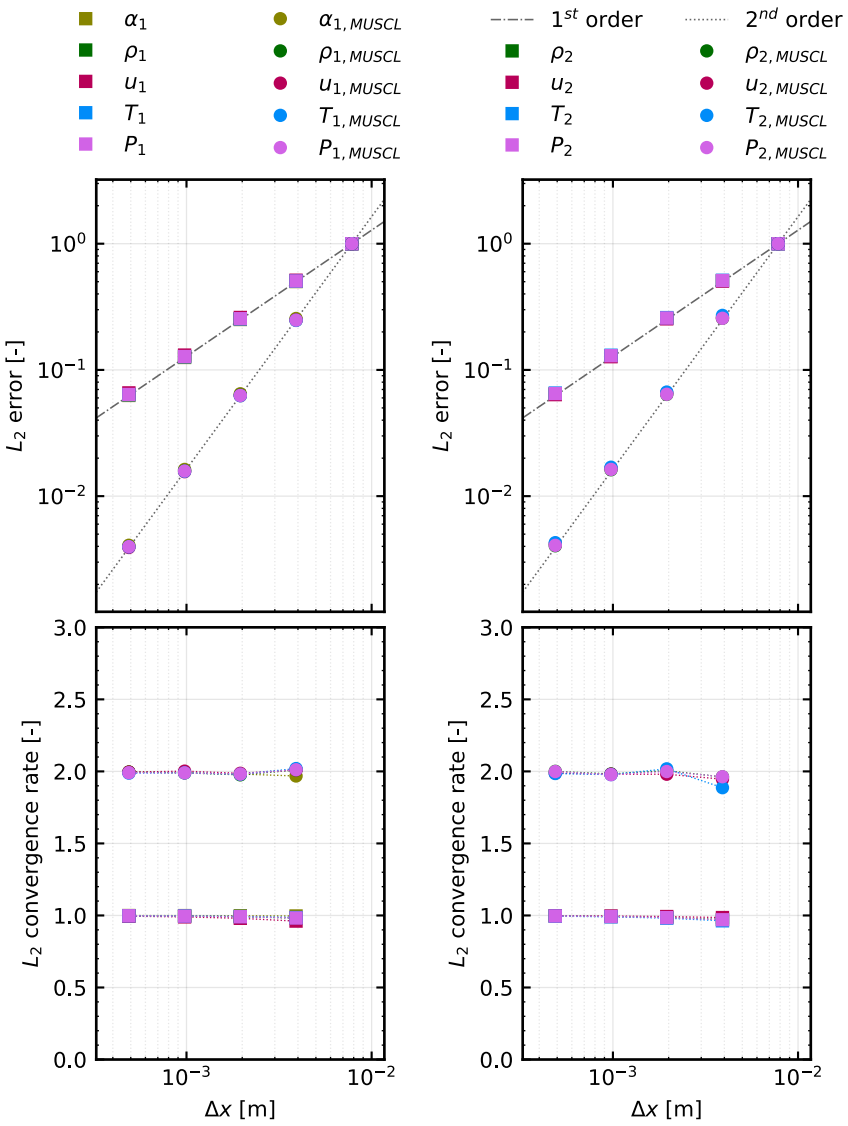

Figure 5: MMS spatial convergence order test for the T update scheme. Dimensionless L_2 norm of the errors and measured convergence rates for volume fraction and phasic densities, velocities, temperatures and pressures. Results for phase 1 are on the left and for phase 2 on the right.

	Phase 1 (SW)	**Phase 2** (SW)	*Time*	$CFL = 1$	$t_{final} = 0.5$ ms
Fluid	MM Vapour [43]	MM Liquid [43]	*Space*	$x \in [0, 1]$ m	$\Delta x = 1$ mm

		Left $x < 0.5$ m		**Right** $x \geq 0.5$ m	
		Phase 1	**Phase 2**	**Phase 1**	**Phase 2**
α	[–]	$1 - 10^{-5}$	10^{-5}	10^{-5}	$1 - 10^{-5}$
ρ	[kg/m^3]	150	700	50	700
u	[m/s]	-50	-50	0	0
P	[bar]	20	20	10	10

Table 7: Non-ideal two-phase MM Riemann problem with the Span-Wagner equation of state. Initial conditions, thermodynamic and numerical data.

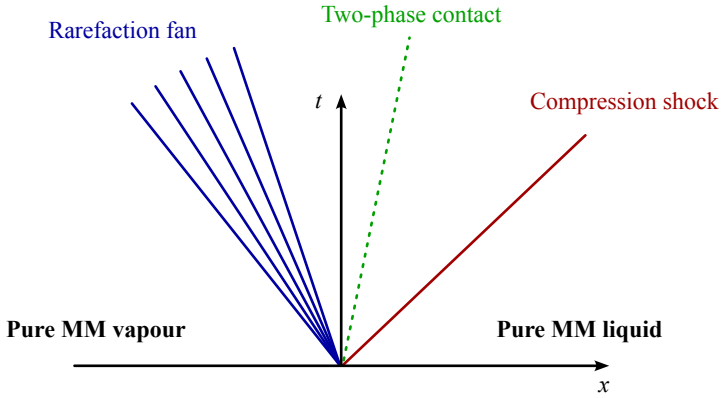

Figure 6: Non-ideal two-phase MM Riemann problem with the Span-Wagner equation of state, sketch of the solution wave structure.

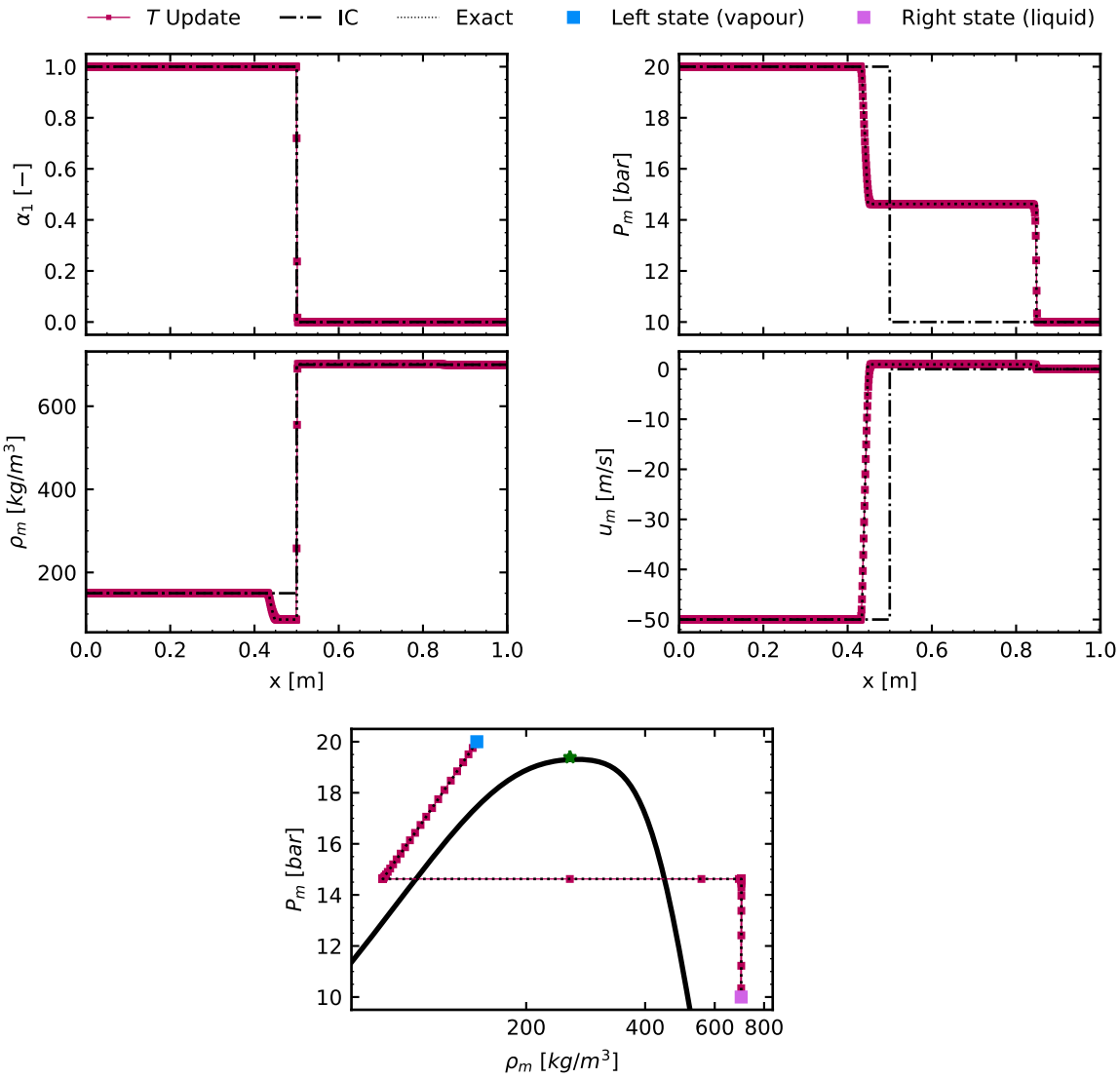

Figure 7: Non-ideal two-phase MM Riemann problem with the Span-Wagner equation of state, using the Coolprop [29] thermodynamic library. Mixture pressure, velocity, density and vapour volume fraction are plotted at $t = 0.5$ ms are plotted. The results are also plotted on the density-pressure thermodynamic plane where the saturation curve is plotted in black and the critical point in green. Comparison between the T update scheme with instantaneous mechanical relaxation and the exact solution.

	Phase 1 (SW)	**Phase 2** (SW)	*Time*	$CFL = 1$	$t_{final} = 2.5$ ms
Fluid	Toluene Vapour [47]	MD_4M Vapour [46]	*Space*	$x \in [0, 1]$ m	$\Delta x = 1$ mm

		Left $x < 0.2$ m		**Right** $x \geq 0.2$ m	
		Phase 1	**Phase 2**	**Phase 1**	**Phase 2**
α	[–]	10^{-5}	$1 - 10^{-5}$	$1 - 10^{-5}$	10^{-5}
ρ	[kg/m^3]	20	340	8	35
u	[m/s]	0	0	50	50
P	[bar]	10	10	3.45	3.45

Table 8: Non-classical MD_4M-Toluene Riemann problem with the Span-Wagner equation of state Initial conditions, thermodynamic and numerical data.

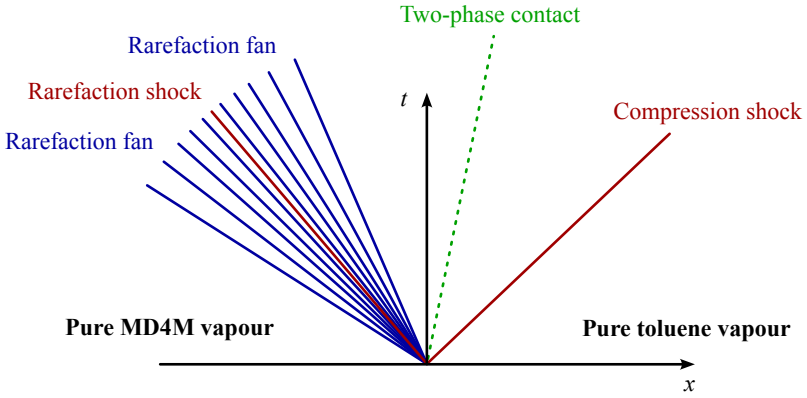

Figure 8: Non-classical MD_4M-Toluene two-fluid Riemann problem with the Span-Wagner equation of state, sketch of the solution wave structure.

non-classical composite rarefaction wave, a two-phase contact separating the MD_4M vapour and Toluene vapour, and a right running compression shock in Toluene vapour. The left-running composite wave is a result of the MD_4M vapour crossing the non-classical gas-dynamics region where the fundamental derivative of gas-dynamics $\Gamma = 1 + \rho c \left(\partial c / \partial P\right)_s$ goes below zero. Starting from the left in Fig. 8, the isentropic rarefaction fan's characteristics start "folding" as they near the $\Gamma < 0$ region, until they match the speed of the double-sonic-shock [44, 45]. This rarefaction shock satisfies the $\Delta s > 0$ condition due to the rarefaction branch of the Rankine-Hugoniot curve crossing the $\Gamma < 0$ region. At the right side of the double-sonic-shock, another isentropic rarefaction fan starts when the characteristics that were previously "folding" match the shock speed again. Note that the SW EoS used here for MD_4M [46] is based on data that is valid only up to, roughly, the critical point. Since the goal of this test is not to validate the scheme against experimental results, but only compare against analytical solutions, we will accept this extrapolation. Plots of the volume fraction, mixture pressure, density and velocity in Fig. 9 show great agreement between the numerical and exact solution, even across the complex non-classical wave located in $x \in [0.07, 0.25]$ m. Results plotted on the thermodynamic planes for MD_4M and Toluene confirm the accuracy of the solution, and the formation of the double-sonic rarefaction shock at $x \simeq 0.15$ m can be best appreciated in the mixture density plot.

4 Conclusions

We presented a mixture-conservative temperature update scheme for the full Baer-Nunziato partial total energy equation. The scheme is valid for arbitrary equations of state and spatial discretization. We showed that the time evolution of the mixture total energy imbalance retains the same behavior as the standard partial total energy update scheme on various 1D Riemann problems from the literature and also when employing complex thermodynamic models such as the Span-Wagner EoS. Furthermore, the pressure-velocity non-disturbance condition remains satisfied. We showed using the van der Waals EoS that the convergence order of the spatial discretization is retained for both first and second order with

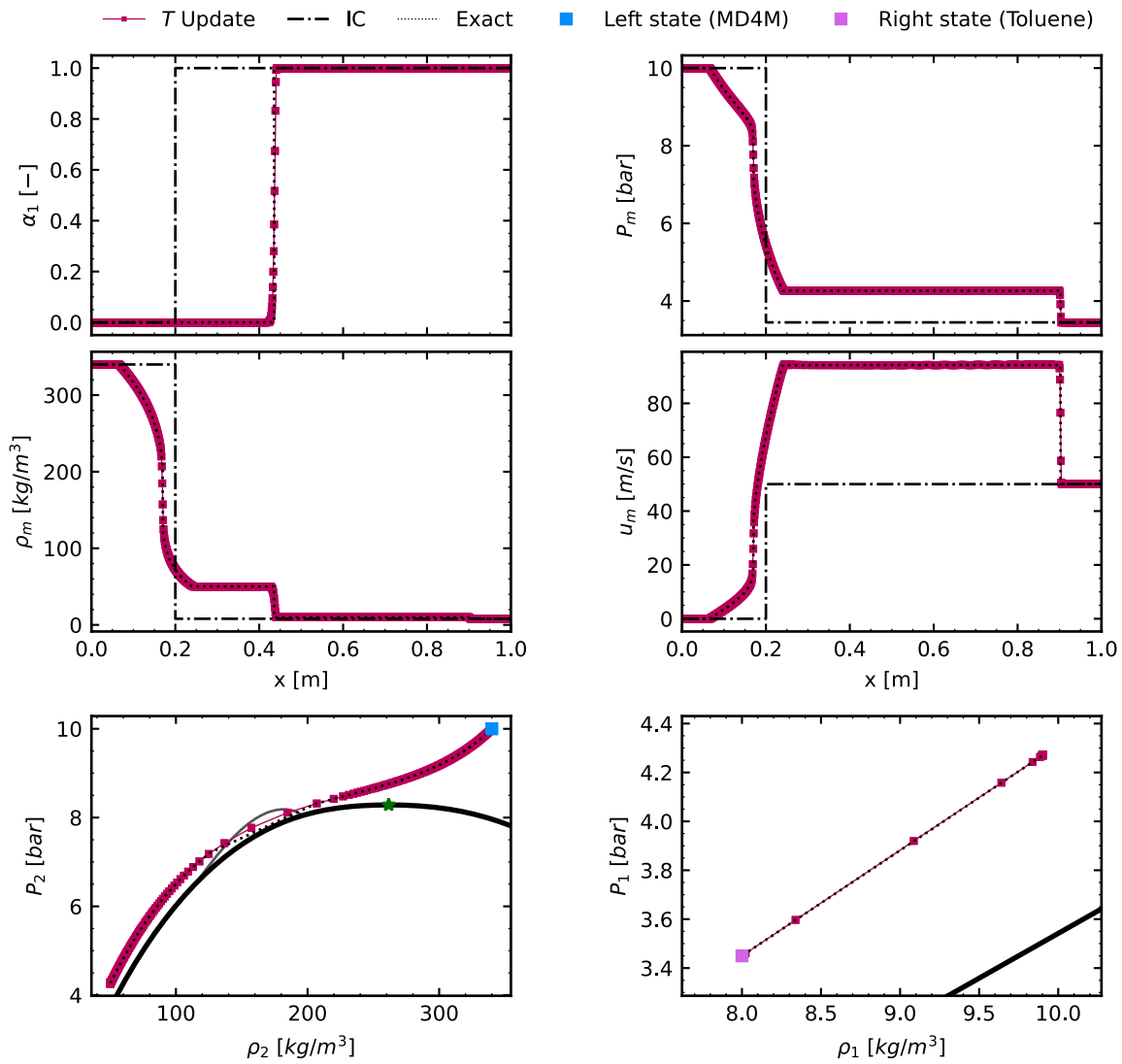

Figure 9: Non-classical MD_4M-Toluene two-fluid Riemann problem with the Span-Wagner equation of state. Mixture pressure, velocity, density and toluene volume fraction are plotted at $t = 2.5$ ms. Comparison between the T update scheme with instantaneous mechanical relaxation and the exact solution. Results on the ρ-P thermodynamic planes are plotted for each phase only where the corresponding volume fraction is above 0.99. The saturation curves are plotted in black, the $\Gamma = 0$ isoline for MD_4M in grey and the critical point for MD_4M in green.

reconstruction. The proposed scheme works well also in two vanishing phase Riemann problems with instantaneous mechanical relaxation in the non-ideal regime, including non-classical wave configurations. The measured computational speed-up of 440% is lower than the expected 700% measured in a similar scheme for single-phase flows developed in a previous work. This is due to the reconstruction of phasic pressures instead of phasic temperatures, required to preserve the pressure-velocity non-disturbance condition. An alternative reconstruction strategy will be studied in future work.

Acknowledgements

B. Re acknowledges the financial support received by the European Union's Horizon Europe programme under the MSCA-2021-PF grant agreement Id 101066019 (project NI2PhORC). G. Sirianni acknowledges the financial support of the European Union under the NextGenerationEU action. G. Sirianni was partially funded by R. Abgrall's UZH Einrichtungkredit.

Dataset

A dataset containing all the numerical results described in this paper is available on Zenodo [48]. The data will be uploaded after the review process.

References

[1] M.R. Baer and J.W. Nunziato. A two-phase mixture theory for the deflagration-to-detonation transition (ddt) in reactive granular materials. International Journal of Multiphase Flow, 12(6):861–889, 1986.

[2] F. Coquel, T. Gallouët, J. Hérard, and N. Seguin. Closure laws for a two-fluid two-pressure model. Comptes Rendus Mathematique, 334(10):927–932, 2002.

[3] V. Perrier and E. Gutiérrez. Derivation and closure of baer and nunziato type multiphase models by averaging a simple stochastic model. Multiscale Modeling & Simulation, 19(1):401–439, 2021.

[4] R. Abgrall. How to prevent pressure oscillations in multicomponent flow calculations: A quasi conservative approach. Journal of Computational Physics, 125(1):150–160, 4 1996.

[5] C. Parés. Numerical methods for nonconservative hyperbolic systems: a theoretical framework. SIAM Journal on Numerical Analysis, 44(1):300–321, January 2006.

[6] M. Castro, J. Gallardo, and C. Parés. High order finite volume schemes based on reconstruction of states for solving hyperbolic systems with nonconservative products. applications to shallow-water systems. Mathematics of Computation, 75(255):1103–1135, March 2006.

[7] L. Gosse. A well-balanced flux-vector splitting scheme designed for hyperbolic systems of conservation laws with source terms. Computers & Mathematics with Applications, 39(9–10):135–159, May 2000.

[8] S. Tokareva and E. Toro. Hllc-type riemann solver for the baer–nunziato equations of compressible two-phase flow. Journal of Computational Physics, 229(10):3573–3604, May 2010.

[9] M. Dumbser and E. Toro. A simple extension of the osher riemann solver to non-conservative hyperbolic systems. Journal of Scientific Computing, 48(1–3):70–88, July 2010.

[10] T. Nguyen and M. Dumbser. A path-conservative finite volume scheme for compressible multi-phase flows with surface tension. Applied Mathematics and Computation, 271:959–978, November 2015.

[11] M. J. Castro, P. G. LeFloch, M. Luz Muñoz-Ruiz, and C. Parés. Why many theories of shock waves are necessary: Convergence error in formally path-consistent schemes. Journal of Computational Physics, 227(17):8107–8129, 9 2008.

[12] R. Abgrall and S. Karni. A comment on the computation of non-conservative products. Journal of Computational Physics, 229(8):2759–2763, 4 2010.

[13] R. Span and W. Wagner. A new equation of state for carbon dioxide covering the fluid region from the triple-point temperature to 1100 k at pressures up to 800 MPa. Journal of Physical and Chemical Reference Data, 25(6):1509–1596, 11 1996.

[14] M. Pini, A. Spinelli, G. Persico, and S. Rebay. Consistent look-up table interpolation method for real-gas flow simulations. Computers & Fluids, 107:178–188, 2015.

[15] A. Guardone, P. Colonna, M. Pini, and A. Spinelli. Nonideal compressible fluid dynamics of dense vapors and supercritical fluids. Annual Review of Fluid Mechanics, 56(Volume 56, 2024):241–269, 2024.

[16] M. De Lorenzo, P. Lafon, M. Di Matteo, M. Pelanti, J.M. Seynhaeve, and Y. Bartosiewicz. Homogeneous two-phase flow models and accurate steam-water table look-up method for fast transient simulations. International Journal of Multiphase Flow, 95:199–219, 2017.

[17] Y. Fang, M. De Lorenzo, P. Lafon, S. Poncet, and Y. Bartosiewicz. An accurate and efficient look-up table equation of state for two-phase compressible flow simulations of carbon dioxide. Industrial & Engineering Chemistry Research, 57(22):7676–7691, 2018.

[18] M. De Lorenzo, P. Lafon, M. Pelanti, A. Pantano, M. Di Matteo, Y. Bartosiewicz, and J.M. Seynhaeve. A hyperbolic phase-transition model coupled to tabulated eos for two-phase flows in fast depressurizations. Nuclear Engineering and Design, 371:110954, 2021.

[19] F.Douglas Swesty. Thermodynamically Consistent Interpolation for Equation of State Tables. Journal of Computational Physic, 127(1):118–127, 1996.

[20] R. Abgrall, P. Bacigaluppi, and S. Tokareva. A high-order nonconservative approach for hyperbolic equations in fluid dynamics. Computers & Fluids, 169:10–22, 2018. Recent progress in nonlinear numerical methods for time-dependent flow & transport problems.

[21] L. Zhang, A. Kumbaro, and J. Ghidaglia. A conservative pressure based solver with collocated variables on unstructured grids for two-fluid flows with phase change. Journal of Computational Physics, 390:265–289, 2019.

[22] B. Re and R. Abgrall. A pressure-based method for weakly compressible two-phase flows under a baer–nunziato type model with generic equations of state and pressure and velocity disequilibrium. International Journal for Numerical Methods in Fluids, 94(8):1183–1232, 5 2022.

[23] A. Thomann and M. Dumbser. Thermodynamically compatible discretization of a compressible two-fluid model with two entropy inequalities. Journal of Scientific Computing, 97(1), August 2023.

[24] R. Abgrall, S. Busto, and M. Dumbser. A simple and general framework for the construction of thermodynamically compatible schemes for computational fluid and solid mechanics. Applied Mathematics and Computation, 440:127629, March 2023.

[25] E. Romenski, A. Resnyansky, and E. Toro. Conservative hyperbolic formulation for compressible two-phase flow with different phase pressures and temperatures. Quarterly of Applied Mathematics, 65(2):259–279, April 2007.

[26] E. Romenski, D. Drikakis, and E. Toro. Conservative models and numerical methods for compressible two-phase flow. Journal of Scientific Computing, 42(1):68–95, July 2009.

[27] G. Sirianni, A. Guardone, B. Re, and R. Abgrall. An explicit primitive conservative solver for the euler equations with arbitrary equation of state. Computers & Fluids, 279:106340, 2024.

[28] R. Abgrall. Staggered schemes for compressible flow: A general construction. SIAM Journal on Scientific Computing, 46(1):A399–A428, 2024.

[29] I. H. Bell, J. Wronski, S. Quoilin, and V. Lemort. Pure and pseudo-pure fluid thermophysical property evaluation and the open-source thermophysical property library coolprop. Industrial & Engineering Chemistry Research, 53(6):2498–2508, 2014.

[30] P. J. Roache. Verification and Validation in Computational Science and Engineering. Hermosa Publishers, 1998.

[31] J. D. van der Waals. The Equation of State for Gases and Liquids. In Nobel Lecture. NobelPrize.org, 1910.

[32] H. A. Bethe. On the theory of shock waves for an arbitrary equation of state. In Classic Papers in Shock Compression Science, pages 421–495. Springer New York, 1942.

[33] Y. B. Zeldovich. 14. on the possibility of rarefaction shock waves. In Selected Works of Yakov Borisovich Zeldovich, Volume I, pages 152–154. Princeton University Press, 12 1946.

[34] P. A. Thompson. A fundamental derivative in gasdynamics. Physics of Fluids, 14(9):1843, 1971.

[35] H. Lochon, F. Daude, P. Galon, and J. Hérard. HLLC-type Riemann solver with approximated two-phase contact for the computation of the Baer-Nunziato two-fluid model. Journal of Computational Physics, 2016.

[36] D.W. Schwendeman, C.W. Wahle, and A.K. Kapila. The riemann problem and a high-resolution godunov method for a model of compressible two-phase flow. Journal of Computational Physics, 212(2):490–526, 2006.

[37] T. Barth and D. Jespersen. The design and application of upwind schemes on unstructured meshes. In 27th Aerospace Sciences Meeting. American Institute of Aeronautics and Astronautics, 1 1989.

[38] N. Andrianov and G. Warnecke. The riemann problem for the baer–nunziato two-phase flow model. Journal of Computational Physics, 195(2):434–464, 2004.

[39] S. Chiocchetti and C. Müller. A solver for stiff finite-rate relaxation in baer–nunziato two-phase flow models. In G. Lamanna, S. Tonini, G. Cossali, and B. Weigand, editors, Droplet Interactions

and Spray Processes, pages 31–44, Cham, 2020. Springer International Publishing.

[40] N. Andrianov, R. Saurel, and G. Warnecke. A simple method for compressible multiphase mixtures and interfaces. International Journal for Numerical Methods in Fluids, 41(2):109–131, 2003.

[41] R. Span, E. Lemmon, R. Jacobsen andW. Wagner, and A. Yokozeki. A Reference Equation of State for the Thermodynamic Properties of Nitrogen for Temperatures from 63.151 to 1000 K and Pressures to 2200 MPa. Journal of Physical and Chemical Reference Data, 29(6):1361–1433, 11 2000.

[42] R. Span and W. Wagner. A New Equation of State for Carbon Dioxide Covering the Fluid Region from the Triple-Point Temperature to 1100 K at Pressures up to 800 MPa. Journal of Physical and Chemical Reference Data, 25(6):1509–1596, 11 1996.

[43] M. Thol, F.H. Dubberke, G. Rutkai, T. Windmann, A. Köster, R. Span, and J. Vrabec. Fundamental equation of state correlation for hexamethyldisiloxane based on experimental and molecular simulation data. Fluid Phase Equilibria, 418:133–151, 2016. Special Issue covering the Nineteenth Symposium on Thermophysical Properties.

[44] C. Zamfirescu, A. Guardone, and P. Colonna. Admissibility region for rarefaction shock waves in dense gases. Journal of Fluid Mechanics, 599:363–381, 2008.

[45] D. Vimercati, G. Gori, and A. Guardone. Non-ideal oblique shock waves. Journal of Fluid Mechanics, 847:266–285, 5 2018.

[46] M. Thol, M.A. Javed, E. Baumhögger, R. Span, and J. Vrabec. Thermodynamic properties of dodecamethylpentasiloxane, tetradecamethylhexasiloxane, and decamethylcyclopentasiloxane. Industrial & Engineering Chemistry Research, 58(22):9617–9635, 2019.

[47] E. Lemmon and R. Span. Short fundamental equations of state for 20 industrial fluids. Journal of Chemical & Engineering Data, 51(3):785–850, 2006.

[48] G. Sirianni, B. Re, and R. Abgrall. Mixture-Conservative Temperature-Based Baer-Nunziato Solver for Efficient Full-Disequilibrium Simulations of Real Fluids: Dataset. Zenodo, 4 2024.